Investigation of Asymmetric Plasma Blob Dynamics

by

Alexander Soane

Submitted to the Department of Physics
in partial fulfillment of the requirements for the degree of

Bachelor of Science in Physics

at the

MASSACHUSETTS INSTITUTE OF TECHNOLOGY

February 2009

Author .....
Department of Physics
January 16, 2009

Certified by....
Jan Egedal
Assistant Professor
Thesis Supervisor

Accepted by .....
David E. Pritchard
Senior Thesis Coordinator, Department of Physics

Investigation of Asymmetric Plasma Blob Dynamics

by

Alexander Soane

Submitted to the Department of Physics
on January 16, 2009, in partial fulfillment of the
requirements for the degree of
Bachelor of Science in Physics

Abstract

The dynamics of asymmetric blobs is investigated in the Versatile Toroidal Facility (VTF) at MIT. Blobs are local regions of enhanced plasma density. Blobs are relevant to several areas of physics research, including fusion experiments. Understanding blob dynamics is important because blobs affect plasma confinement, a key issue for fusion experiments. The blobs in this experiment are created under varying magnetic and neutral gas density conditions. We explore several methods for creating these asymmetric blobs and offer theoretical predictions for some of the behavior. Four arrays of Langmuir probes are placed inside the toroidal chamber to measure plasma density. Data collected is shown to confirm the existence of a plasma blob and is analyzed to extract radial and toroidal information. Radial propagation is compared with a previous experiment that featured symmetric blobs. We find that the presence of a vertical magnetic field is a significant variable for radial speed. Toroidal motion is shown to be very fast relative to the radial propagation. This experiment serves as a useful reference for future research on asymmetric blobs.

Thesis Supervisor: Jan Egedal
Title: Assistant Professor

Acknowledgments

Over the course of this thesis, several individuals have contributed to my success and happiness. I would like to acknowledge their contributions by extending a special thanks to Professor Jan Egedal, Noam Katz, mon ami Ari Lê, Arturs Vrublevskis, Jeffrey Bønde, Will Fox, Brian Kardon, Drs. Zoya and David Soane, Nicky Soane, Matthew Schram, Willian Uspal, Christopher Leon, Conner Galloway, Alex Valys, John Michaels, Dr. Abhay Ram, Basshunter, Pakito, Alizée, and Armin van Buuren.

Contents

List of Figures

List of Tables

Chapter 1

Introduction

Plasma, as the fourth state of matter, comprises the vast majority of our visible universe. The most primitive definition of plasma, that of a dissociated, charged classical gas, implies a wide range of fascinating and complicated dynamics. Charged particles respond to electromagnetic fields. In turn, the motion and distribution of charged particles establish time dependent electromagnetic fields. We find that plasma is a self-interacting entity, subject to all of the relevant classical physics such as thermodynamics and turbulence.

Plasma filaments, also known as "blobs", are distinct structures encountered in plasma environments. Blobs are coherent structures, described as a local increase in plasma density along a magnetic field line relative to the background. In general, blobs are independent entities, and normally acquire a unique temperature relative to the rest of the system. Consequently, the dynamics that govern plasma blobs may also be different; for example, blob motion is convective as opposed to diffusive. Because plasma blobs are present in all plasma environments, ranging from the planetary scale to that of Earth-based fusion experiments, understanding the physics that governs blob dynamics will be significant [6, 5, 4].

Blob propagation has been theoretically investigated in depth, owing to the fact that blob propagation negatively affects plasma confinement. Although several aspects of blob propagation, such as scaling relations, are now theoretically predicted, there is a lack of direct experimental observation of blob propagation in the literature. This deficiency of experimental evidence is principally due to the fact that conditions for fusion plasma prohibit the use of internal probes.

In this thesis, I present experimental observations of toroidally asymmetric plasma blobs, created by using the resources of the Versatile Toroidal Facility (VTF) of the Plasma Science and Fusion Center (PSFC) at MIT. In particular, the measurements were conducted by using internal probes, a unique feature that the particular configuration of the VTF makes possible. The physical description of toroidally asymmetric blobs is compared to the experimental results of a prior study by students at VTF. Their work is published in Katz et al [2]. In this study, the authors looked at the effect of neutral gas on the propagation and structure of a toroidally symmetric blob ("filament"). Because the two blob structures have different degrees of freedom (asymmetric versus symmetric), we expect to discover interesting new properties in the case of asymmetric blobs.

This thesis is organized as follows. I will apply basic plasma principles to formulate an underlining theory of radial blob propagation as well as to offer some predictions for asymmetric blobs. Subsequently, I will review the experimental setup and data collection scheme. Calibration will be discussed as an introduction to the raw data. Data analysis and results will be presented along with some physical interpretations. Commentary for future research will conclude this thesis.

Chapter 2

Experimental Setup

2.1 Versatile Toroidal Facility

Originally a tokomak, the Versatile Toroidal Facility (VTF) is a device used to create a plasma environment [1]. The main chamber is toroidal with a square cross section and dimensions given in Fig. 2-1. During normal operation, the VTF chamber is vacated. Plasma is created by ionizing a low-pressure Argon gas that fills the vacuum chamber. Throughout this thesis, references to the "vacuum" assume some known, low-density neutral Argon gas. Neutral Argon pressure was consistently on order of 10^{-4} torr, which is substantially lower than atmospheric pressure. This chamber-filling Argon gas was ionized with RF energy to create a plasma. In order to ionize Argon, a background magnetic field of appropriate magnitude must be established. This field is in the toroidal direction and is created by eighteen large coils that are spaced evenly around the chamber at separations of 20 degrees. Electromagnetic power is provided by a 2.45 GHz, 15 kW microwave source. This energy is directed into the vacuum chamber via a waveguide horn, located at toroidal angle 260 degrees. The relative location of the microwave horn to the other equipment of interest is shown

in Fig. 2-2. In addition to the large external coils necessary to establish the toroidal magnetic field, vacuum-sealed ports on the sides of the VTF vessel give access to the interior of the vacuum chamber. This enables the placement of probes for collecting data and externally-controlled coils for changing the local magnetic field profile. A photograph of the VTF apparatus is shown in Fig. 2-2.

2.2 Plasma Blob Creation by an Interior Coil

Under the conditions in the VTF, the strength of an applied magnetic field needs to be ≈ 87 mT for the electron cyclotron motion to be resonant with the RF power. This is the condition for ionizing the Argon gas to create a plasma. The eighteen external coils create a large toroidal magnetic field, which in turn may be augmented by a wide assortment of small coils. The strength of the toroidal field (background field) allows us to manipulate the local magnetic field strength with smaller coils of specific geometry. For example, a toroidally symmetric coil placed on the inner wall of the chamber may be used to create a net magnetic field strength of 87 mT at the inner wall. Due to the sensitivity of the Argon gas to the precise ionization condition, any perturbative field that brings the net local strength to 87 mT governs the location and three dimensional structure of an emerging plasma, given that neutral Argon gas is uniformly distributed inside the chamber. In particular, this fact may be readily exploited to create a region of localized, high density plasma called a blob.

As an example, we may consider the toroidally symmetric blobs used by Katz et al [2]. In their experiment, the authors used a toroidally symmetric coil mounted on the inner wall inside the vacuum chamber in conjunction with the external, toroidal coils. This configuration created a toroidal ring on the inner wall of the chamber where the magnetic field reached 87 mT. Thus, a plasma "donut" (toroidally symmetric blob) was formed at the inner wall. This symmetric blob (sometimes referred to as

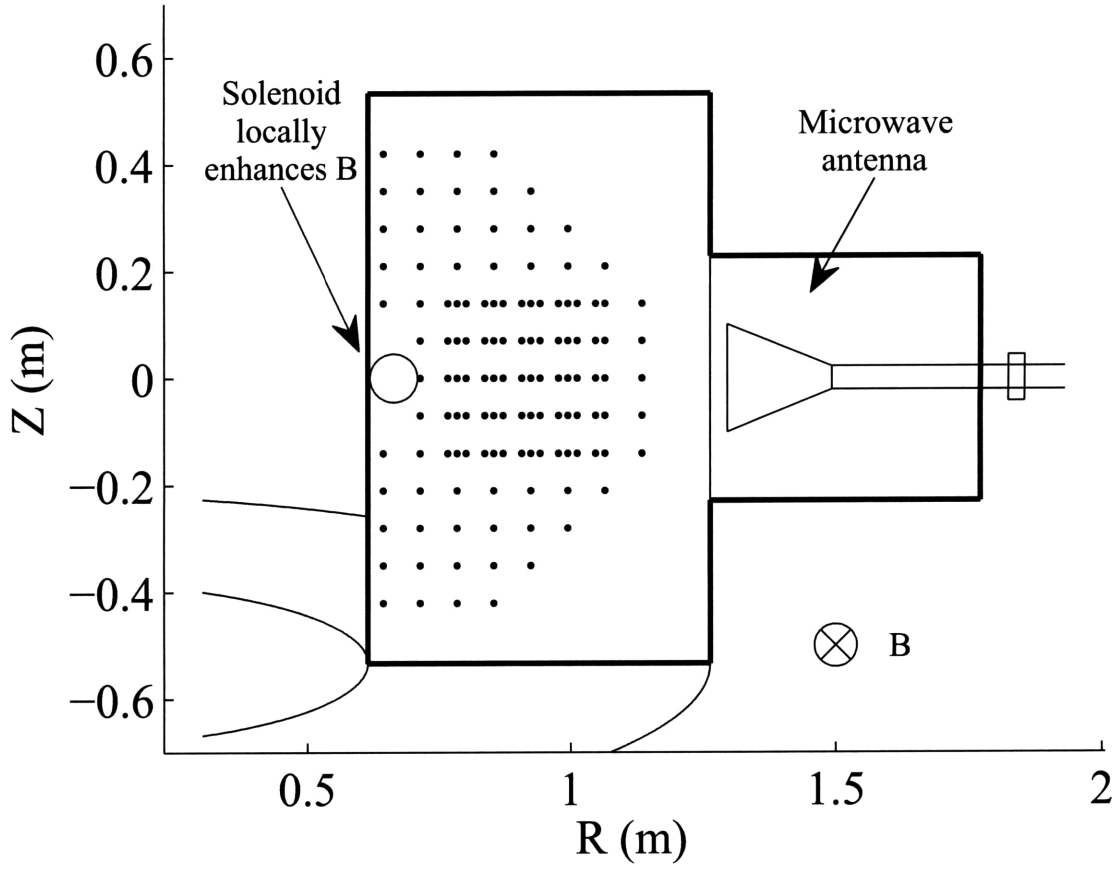

Figure 2-1: This diagram is representative of how the inside of the vacuum chamber appears. Microwaves emitted from the horn ionize neutral gas near the interior toroidal wall. The perturbative coil produces a net field of 87 mT that is necessary for ionization. The dots represent Langmuir probes. For the experiment described in this thesis, the probes are located at different toroidal angles and in a square pattern.

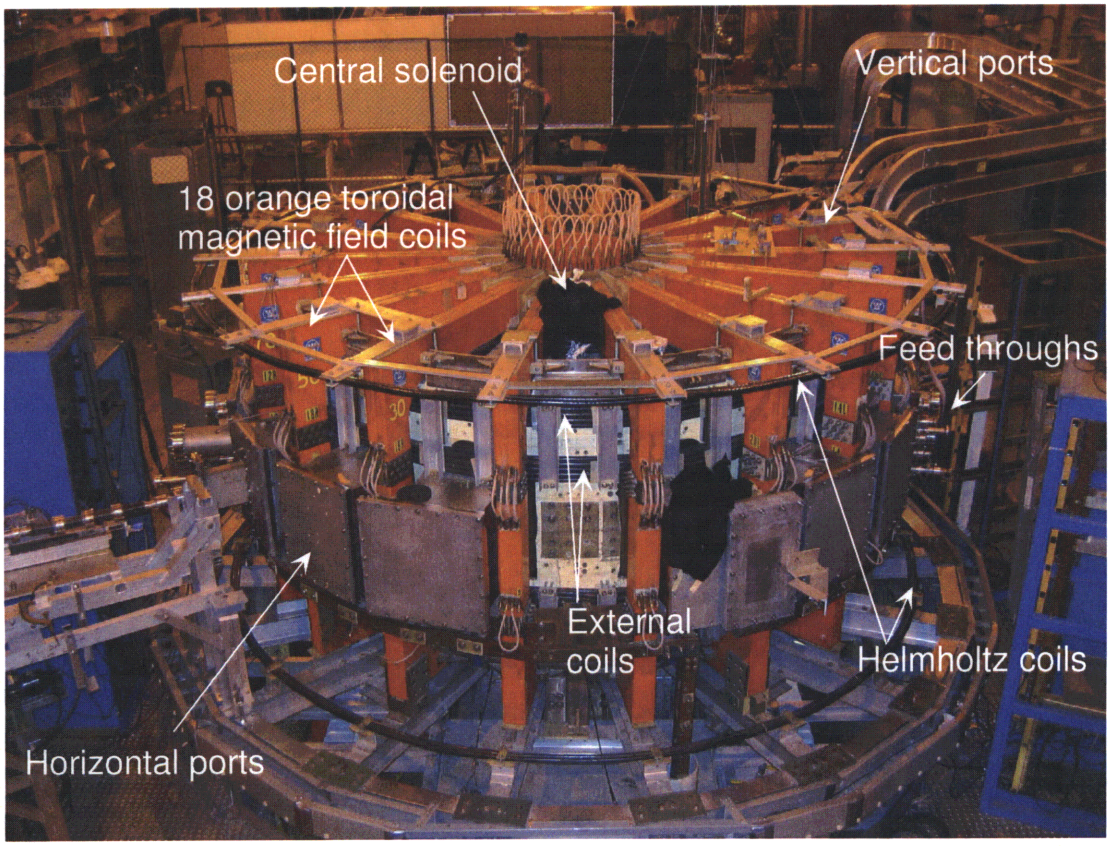

Figure 2-2: A photograph of the exterior of the VTF plasma machine, illustrating the layout of equipment and the vacuum vessel.

a "filament" in the literature) was subsequently manipulated by changing additional parameters in the system, such as neutral gas density.

In this thesis, the properties of an asymmetric blob were investigated. Thus, a fundamental component of the thesis involved generating an asymmetric blob. Inspired by the technique used to create a symmetric filament, an asymmetric blob could potentially be generated by using a small coil. In the case of the symmetric blobs, the coil was large and situated completely around the inner wall of the chamber. A small coil, located at one angular cross section inside the chamber, forms an asymmetric system. Combined with the toroidal background field, a pulsed current through the perturbative coil creates a region of space inside the chamber where the ionization condition is met. In contrast to the symmetric scenario, the ionization condition is confined to a small toroidal distribution, which would cause a toroidally localized blob to form.

The coil used contained twenty four turns, partitioned into four different loops at right angles to each other, like a cross. Each loop had a diameter of 10 cm. The coil was supplied by an external circuit that featured a 4.5 mF capacitor bank charged to $\sim$ 130 V. An SCR diode controlled the current pulse, triggered by a 5 V logic signal. This same SCR diode shorted the coil to itself from ground, thus preventing normal LC oscillations from harming the polarized capacitors. The peak current through the coil was over 1 kA, which corresponded to a calculated $\sim$ 50 mT peak in the local magnetic field. Coupled with the toroidal background field, the net strength exceeded 87 mT. Thus, the ionization condition was met at some time during the current pulse in the coil. The coil was placed at a toroidal angle of 240 degrees, near the microwave horn. The close proximity to the horn would optimize the ionization procedure and facilitate the creation of an asymmetric blob.

A controlled, asymmetrically located coil provides some experimental advantages. Because the coil provides $\sim$ 50 mT of magnetic field, the background toroidal field

strength may be reduced to a fraction of 87 mT, the ionization condition. Interesting physics may occur for a low-field plasma. Experiments that use the asymmetric blobs created with a small coil may be able to probe the regime of low-field plasmas because a strong toroidal field is unnecessary to generate plasma.

2.3 Plasma Blob Creation by Direct Injection of Argon Gas

An alternative method for generating toroidally asymmetric blobs centered on using localized puffs of Argon gas into a background vacuum of some nominal neutral pressure. Argon puffs were achieved by using logic-controlled, piezoelectric valves located at the inner wall of the chamber. Because the valves were located at specific toroidal angles, the asymmetry in the system was introduced by injecting the Argon gas at these distinct angles. In order to satisfy the 87 mT ionization requirement, two different coils were used. The exterior toroidal coils provided $\sim$ 50 mT. An interior, toroidal coil was located at the inner wall. This coil was pulsed such that the net magnetic field strength near the inner wall reached 87 mT. The interior coil was used to prevent the entire vacuum chamber from reaching 87 mT. Such a situation would allow gas to ionize throughout the entire chamber, which would ruin the formation of a distinct plasma blob. Although the net field was toroidally symmetric, the asymmetic Argon puff would become a higher density plasma than the background when microwaves were introduced into the chamber. In the specific VTF setup, the piezoelectric valve used was at toroidal angle 270 degrees, near the microwave horn. To successfully create a localized blob, the piezoelectric valve is opened for $\approx$ 1 ms. This activation overlaps with radiation of microwave energy through the horn. Ionized plasma, supplied with microwave energy, can ionize incoming neutral Argon from the

valve. In this way the plasma blob retains its asymmetric feature.

When the Argon puff method is applied to generate an asymmetric blob, the symmetric toroidal field must be $\sim$ 87 mT for the ionization condition to be satisfied. The inner coil alone cannot reach this requirement. This precludes the experimental design from reaching low-field parameters, which in the method described in Chapter 2.2 would be provided principally by the strong, toroidally asymmetric coil. Conversely, higher-strength fields are now accessible, because the low Argon background density would be a weak plasma compared to the region immediately around the piezoelectric valve.

2.4 Langmuir Arrays

The unique arrangement of the VTF equipment allows for an experimental design that includes direct measurement of plasma by internal probes. For this thesis, the internal probes consisted of four hanging arrays of Langmuir probes. These probes were located at toroidal angles 240, 270, 300, and 340 degrees. The placement of the arrays was optimum for high resolution data of an asymmetric blob created near the microwave horn. The parameters for the four arrays are shown in Table 2.1.

Table 2.1: Langmuir array specifications for the experiment.

Angle	Number	Vertical (meters)	Radial (meters)
240	8×16	$-0.3800 \leftrightarrow 0.3700$	$0.7130 \leftrightarrow 1.2030$
270	16×12	$-0.3465 \leftrightarrow 0.4235$	$0.7040 \leftrightarrow 1.2290$
300	8×16	$-0.3500 \leftrightarrow 0.4000$	$0.7150 \leftrightarrow 1.2050$
340	8×16	$-0.3500 \leftrightarrow 0.4000$	$0.7150 \leftrightarrow 1.2050$

The Langmuir arrays have the property of being able to measure either ion saturation or floating potential. In the former case, the probes are biased negative relative to the plasma in order to collect fewer electrons. The fast electrons normally have a

greater flux than the slow ions. Reducing the probe's potential will lower the electron flux. For a sufficiently negative probe potential, the electron flux will be zero. The potential when there is no electron flux is known as the ion saturation potential. It is possible to extract the ion density by using numerical factors related to the geometry of the probes.

Floating potential is defined by a net zero charge flux on the probe. This is once again a negative potential, because the mass difference between electrons and ions results in different mean speeds for a given plasma temperature. This difference in speeds translates into a difference in charge flux. Consequently, a negative potential is required to bring the electron and ion fluxes into equivalence.

Chapter 3

Theory

The central theme of this thesis is an experimental investigation of toroidally asymmetric plasma blobs. The concept for this thesis arose as a natural extension of an earlier experiment conducted at VTF by Katz et al [2]. This experiment measured toroidally symmetric plasma blobs for the first time using internal probes. A dependence of the radial blob propagation speed on neutral gas density was observed. This observation was derived theoretically from governing magnetohydrodynamics equations. Because asymmetric plasma blobs have several similarities to symmetric blobs, it is instructive to discuss some underlying theory about blob propagation in the context of Katz et al. This theory about blob propagation will be augmented for the generalized case of toroidal asymmetry when I present some hypotheses about asymmetric blobs.

3.1 Symmetric Blob Propagation

In a paper published by Katz et al [2], the authors discuss a theoretical model that explains observations of symmetric blob radial propagation speed. We will give a

brief overview of these results. As detailed in the experimental setup chapter of this thesis (see Chapter 2.2), a symmetric blob may be created by introducing a toroidally symmetric "perturbation" magnetic field over the background toroidal field. By positioning an interior coil around the inner wall of the chamber, the perturbation field is confined to a thin region. With the proper current supplied to the interior coil, the net magnetic field may reach the ionization condition of 87 mT. During a normal experiment run (the term is "shot"), the microwave energy is supplied for $\sim$ 100 microseconds, at the beginning of a data collection run that lasts for milliseconds. All plasma formation occurs during the microwave stage, because energy supplied is used immediately to ionize an entire flux tube of neutral Argon gas.

It is important to understand how the geometry of the magnetic field affects the plasma. The toroidal nature of the field gives rise to curvature and gradient drift. Curvature drift is the effect of a bend in the magnetic field, in this case around the entire chamber. A force balance equation shows that magnetic field curvature results in a change in net velocity:

$$\mathbf{v}_{curv} \propto \frac{1}{q}\mathbf{B} \times (\mathbf{e}_B \cdot \nabla)\mathbf{e}_B. \tag{3.1}$$

Immediately, we recognize that the drift is in opposite directions for ions and electrons because of the factor of q. Furthermore, we know that the alignment of the toroidal field is such that $\mathbf{e}_B = \mathbf{e}_\phi$. Thus, in cylindrical coordinates, the factor

$$(\mathbf{e}_B \cdot \nabla)\mathbf{e}_B = (\mathbf{e}_\phi \cdot \nabla)\mathbf{e}_\phi \tag{3.2}$$

$$\Rightarrow (\mathbf{e}_B \cdot \nabla)\mathbf{e}_B = \frac{1}{r}\frac{\partial}{\partial \phi}\mathbf{e}_\phi \tag{3.3}$$

$$\Rightarrow (\mathbf{e}_B \cdot \nabla)\mathbf{e}_B \sim -\mathbf{e}_r. \tag{3.4}$$

Thus, $\mathbf{e}_B \times \mathbf{e}_r = \mathbf{e}_z$, and we may rewrite Eq. 3.1 as

$$\mathbf{v}_{curv} \sim \frac{1}{q}\mathbf{e}_z. \tag{3.5}$$

Consequently, ions drift in the $\mathbf{e}_z$ direction and electrons opposite, in the $-\mathbf{e}_z$ direction. This leads to a vertical charge separation.

A similar analysis of the magnetic field and force balance equation produces the gradient drift:

$$\mathbf{v}_{grad} \propto \frac{1}{q}\mathbf{B} \times \nabla B. \tag{3.6}$$

Assuming perfect toroidal symmetry in the magnetic field (a good assumption), Ampère's law shows that the only coordinate dependence of B is $B \propto \frac{1}{r}$. Thus, $\nabla B \propto -\frac{1}{r^2}\mathbf{e}_r$ and the gradient drift velocity becomes

$$\mathbf{v}_{grad} \propto \frac{1}{q}\mathbf{B} \times \nabla B \tag{3.7}$$

$$\mathbf{v}_{grad} \sim \frac{1}{q}\mathbf{e}_\phi \times (-\mathbf{e}_r) \tag{3.8}$$

$$\mathbf{v}_{grad} \sim \frac{1}{q}\mathbf{e}_z. \tag{3.9}$$

The effect of the gradient drift is equivalent to the curvature drift: Ions drift in $\mathbf{e}_z$ and electrons in $-\mathbf{e}_z$, which leads to a charge separation in the plasma blob as shown schematically in Figure 3-1.

The vertical separation of charges is important because an electric field $\mathbf{E} \sim -\mathbf{e}_z$ accompanies this charge separation. It is well known that $\mathbf{E} \times \mathbf{B}$ drift is related by:

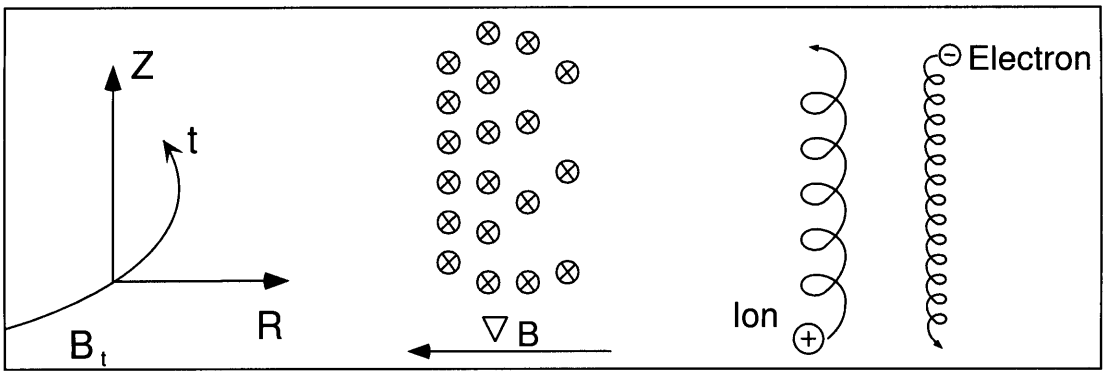

Figure 3-1: Gradient drift causes vertical charge separation.

$$\mathbf{v}_{E\times B} = \frac{\mathbf{E}\times\mathbf{B}}{B^2} \tag{3.10}$$

$$\mathbf{v}_{E\times B} \sim -\mathbf{e}_z \times \mathbf{e}_\phi \tag{3.11}$$

$$\mathbf{v}_{E\times B} \sim \mathbf{e}_r. \tag{3.12}$$

Since there is neither a mass nor charge dependence in Eq. 3.12, the ion and electron radial drift is equal. Thus, the result of crossed electric and magnetic fields in the VTF geometry is a net blob drift radially outward in the chamber cross section. This outward drift is shown schematically in Figure 3-2

We can see a good demonstration of the $\mathbf{E}\times\mathbf{B}$ drift in an experimental measurement from Katz et al [2]. The authors calculate the effective $\mathbf{E}\times\mathbf{B}$ velocity by measuring the potential within the blob. The gradient of the potential yields the electric field. The data are shown in Figure 3-3.

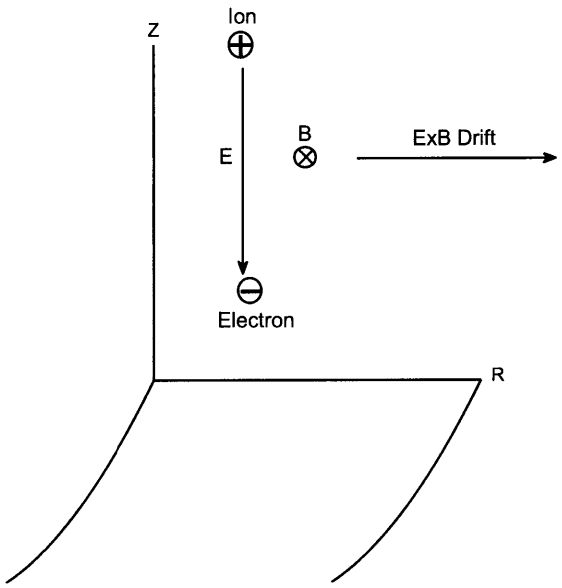

Figure 3-2: E cross B drift is directed radially outward and in equal magnitude for both electrons and ions.

3.2 Blob Slowing

The E cross B drift picture works well for a single particle in crossed fields. A more realistic behavior for propagation blobs needs to take into account the fact that the plasma is comprised of many charged particles and exists in a bath of neutral gas. Statistically governed interactions between particles will contribute to the loss of energy in the blob, which will slow the blob propagation. These interactions can be understood as collisions with neutrals and adiabatic cooling, which we will discuss now.

3.2.1 Collisions with Neutral Gas

The analysis in Chapter 3.1 provides an heuristic understanding for why blobs propagate radially outward. This treatment, however, neglects the neutral gas in the chamber. The principle discovery of Katz et al [2] was the fact that plasma blobs interact with the neutral gas. The authors observed a radial blob speed dependence on neutral pressure as $|\mathbf{v}_r| \propto \frac{1}{P_n}$. They further demonstrated that this behavior may be derived from magnetohydrodynamics (MHD) equations by including a neutral-collision term in the vorticity equation:

$$\nabla \cdot \frac{m_i n}{B^2} \frac{D\nabla_\perp \phi}{Dt} = \nabla_\parallel J_\parallel + \frac{2}{B} \mathbf{b} \times \kappa \cdot \nabla p - \nabla \cdot \frac{m_i n}{B^2} \nu \nabla_\perp \phi. \tag{3.13}$$

Equation 3.13 is a statement about the divergence of current density J being zero, as we will elaborate on below. The symbols $\perp$ and $\parallel$ are defined with respect to the magnetic field. It is important to focus on the term $\nabla_\parallel J_\parallel$ because this is directed along the magnetic field lines. A reasonable assumption in the case of symmetric blobs is that there is no current along the magnetic field by symmetry. Consequently, the current along the magnetic field, $J_\parallel$, is ignored in the calculations.

Further exploiting the symmetric geometry of the experiment, Eq. 3.13 may be simplified:

$$\nabla \cdot \frac{m_i n}{B^2} \frac{D\nabla_\perp \phi}{Dt} = \frac{2}{BR} \frac{dp}{dZ} - \nabla \cdot \frac{m_i n}{B^2} \nu \nabla_\perp \phi. \tag{3.14}$$

R is a characteristic radius, about 1 meter. Similarly, Z is a characteristic vertical position. Other variables are ν, the collision frequency; m_i, the mass of ions; and n, the plasma density. The terms in Equation 3.14 are related to divergence of some currents. The left hand side is the divergence of ion polarization currents known as vorticity accumulation. The first term on the right hand side represents the divergence

of currents due to curvature and magnetic field gradient drifts. The second term is the divergence of Pedersen currents, which is the collisional damping due to neutrals. In addition to the vorticity equation, the continuity equation must be obeyed:

$$\frac{\partial n}{\partial t} + \nabla \cdot (n\mathbf{v}) = 0. \tag{3.15}$$

This is a statement about the conservation of plasma particles (reasonable for times after the microwave source is off). By considering the vorticity and continuity equations simultaneously, it is possible to derive an analytical expression for the average radial velocity of the blobs:

$$\langle v_R \rangle = \frac{2\langle c_s^2 \rangle}{\nu R}, \tag{3.16}$$

where the collision frequency $\nu = n_n \sigma \bar{v}_i$. The sound speed, c_s, is given by $c_s \equiv \sqrt{T_e/m_i}$. Inserting numerical parameters for the VTF, the sound speed is approximately 2 km/s. σ is the collision cross section and $\bar{v}_i$ is the mean ion speed. The mean ion speed is assumed to be much larger than $\langle v_R \rangle$ because the individual ion motion is governed by convective flows and ion temperature. Eq. 3.16 shows that the average blob radial speed scales with the inverse of neutral density, $\frac{1}{n_n}$.

There is a simple heuristic explanation for why neutral gas slows the plasma blob that is taken from [3]. In general, the charge exchange between an ion A^+ and a neutral atom B is

$$A^+_{fast} + B_{slow} \rightarrow A_{fast} + B^+_{slow}. \tag{3.17}$$

There is minimal momentum transfer in this process because the Coulomb interaction between the ion and valence electron of the neutral is much stronger than the interaction between the nuclei. Consequently, the net effect is to evaporate some

energy from the plasma blob via the escaping, newly born neutral after the charge transfer. The new ion is to good approximation at rest relative to the plasma blob. Due to the $\mathbf{E} \times \mathbf{B}$ force inside the blob, the slow ion is gradually accelerated radially. By this process the blob speed is regulated by slow neutral gas particles. We see that over time, the blob loses speed as energy is evaporated by newly born fast neutrals.

On a larger scale, the charge exchange between fast ions and slow neutrals is manifested as a drag force. This drag force is equal to the centrifugal force of the orbiting particles. Essentially, the electric field may be thought of as a mediator between centrifugal and drag forces.

In deriving Eq. 3.16, some assumptions were made about the geometry of the experiment. As mentioned earlier, the toroidal symmetry is a luxury that by definition asymmetric blobs do not have. Asymmetries introduced may affect the velocity scaling law. The experimental observation of disparities between symmetric and asymmetric blob behavior is the focus of this thesis.

3.2.2 Adiabatic Cooling

The process of adiabatic cooling leads directly to blob energy loss. As the flux tube expands radially, it encloses greater volume. The decrease in local plasma density within the blob is related to the adiabatic expansion of a thermodynamic piston. Consequently, with increasing radius, the blob speed should decrease. This behavior is present in both symmetric and asymmetric blobs, albeit with different levels of importance. The symmetric blob will certainly occupy greater volume with increasing radius; however, the asymmetric blob must also undergo toroidal expansion in addition to radial expansion. A consequence of this disparity in expansion volume is that the asymmetric blob will lose a greater amount of energy to adiabatic cooling.

Because the temperature of a plasma is related to the average particle velocity,

cooling the plasma will slow the orbiting particles. The consequence of this is a reduced centrifugal force, which leads to a weaker electric field and thus slower radial drift.

3.3 Asymmetric Blob Predictions

3.3.1 Initial Setup

One of the fundamental open questions about asymmetric blobs is whether or not the toroidal propagation exhibits coupling to the environment in a manner similar to symmetric blobs. We describe several contingencies for a variety of possible effects that may be seen in the experiment. An intuitive hypothesis is that toroidal propagation of plasma is confined to flux tubes and expands at the sound speed. In other words, that the toroidal flow is purely convective and independent of neutral gas. However, results from symmetric blob radial propagation show the importance of neutral gas, a discovery that may change our expectations of toroidal blob expansion. A key feature of the asymmetric blob experimental setup is that the magnetic field inside the vacuum chamber is confined to a narrow angular section. Ideally, plasma formation at angles far from the region of 87 mT is due to plasma collision with neutral gas as the plasma expands toroidally. This is in contrast to the symmetric blob case, in which all toroidal angles ideally met the ionization condition and plasma formation was uniform. Consequently, we may expect to observe a dependence of toroidal speed on neutral gas density that is due to the charge-transfer collision between ion and atom not exchanging momentum, a process described by Eq. 3.17.

If there is a toroidal speed dependence on neutral gas density, we may expect that in the low pressure limit the toroidal speed approaches the sound speed, c_s. To test the experimental setup, we take the case of a high angular confinement for

the neutral Argon puff. Assuming $c_s \approx 2000$m/s and an average toroidal radius of $R \approx 1$m, an upper bound on the toroidal propagation time is $\Delta t_\Phi = \frac{1}{2}\frac{2\pi R}{c_s} \approx 1.5$ms. The factor of $\frac{1}{2}$ is included because opposite toroidal ends of the blob propagate symmetrically. 1.5ms is on the order of the time interval commonly used during data collection, so the experimental setup is well designed to detect a toroidal spread under these assumptions. However, if the gas puff has a wide angular spread or the electrons are significantly hotter than the 2eV incorporated in the stated c_s, then toroidal spread may be fast. For example, for electrons at a temperature of 10eV, the sound speed is $c_s = 2000\sqrt{\frac{10}{2}} \approx 4500$m/s. Additionally, we are limited in angular resolution by a spread of 100 degrees between the outer langmuir arrays. Noting that the both the piezoelectric gas valve and the microwave horn are centrally located with respect to the available measured angles, blob formation that extends beyond the Langmuir arrays is possible. If we combine increased sound speed with a plasma blob spread over 150 degrees (already outside of our angular resolution) and a more accurate radius of 0.625m, then the time for the blob to connect on itself toroidally is $\Delta t_\Phi = \frac{1}{2}\frac{210}{360}\frac{2\pi(0.625)}{4500} \approx 250\mu$s. This is on the order of the microwave heating time of $\sim 75\mu$s, a period of significant data pollution by plasma ionization and fast flows. The message is twofold: Angular resolution limits our measurement of toroidal propagation and hot electrons significantly reduce the spreading time. An experimental solution to the problem of measuring toroidal spread needed to be found.

3.3.2 Introducing a Vertical Component to the Magnetic Field

The principle reason for why increased electron temperature and blob width could influence the observations is the vertical independence of the original setup. In the absence of a vertical component to the magnetic field, flux tubes are confined to a

single horizontal plane. Thus, the maximum length of a flux tube is the circumference of the VTF chamber. As shown, plasma propagation through this circumference is potentially too fast to be statistically regarded as accurate data. A simple solution to the conundrum was to introduce a small vertical component to the otherwise toroidal magnetic field. The helical geometry of the magnetic field would effectively triple or quadruple the total length of flux tubes as well as prevent then from closing on themselves. Watching an individual cross section would be the equivalent of probing several passes around the chamber because field lines intersect the cross section at different vertical positions. The vertical separation at given radius is computed:

$$\Delta z(r) = \frac{\Theta r B_z}{B(r)} = \frac{2\pi r^2 B_z}{B_o R} \tag{3.18}$$

where R is the characteristic radius 1m, B_z is the z component of the magnetic field, and B_o is the magnitude of the total field. The second step involves setting $\Theta = 2\pi$ and associating $B(r) \sim B_o \frac{R}{r}$. Eq. 3.18 shows that flux tubes, viewed in a cross section, appear to spread vertically (positive or negative based on the propagation direction around the chamber) with a quadratic dependence on radius. This predicts a tracking scheme for monitoring the toroidal spread of the asymmetric blob. A new signal should appear on the Langmuir arrays for each toroidal pass of the blob at a predictable coordinate. Even assuming a sound speed of 4500m/s, three complete orbits around the chamber would need on the order of 1ms to complete, which is on the timescale of the radial propagation. Motivated by the preceding calculations, we introduced the vertical magnetic field as an additional parameter for the experiment. Thus, our experimental variables are neutral gas pressure and vertical magnetic field.

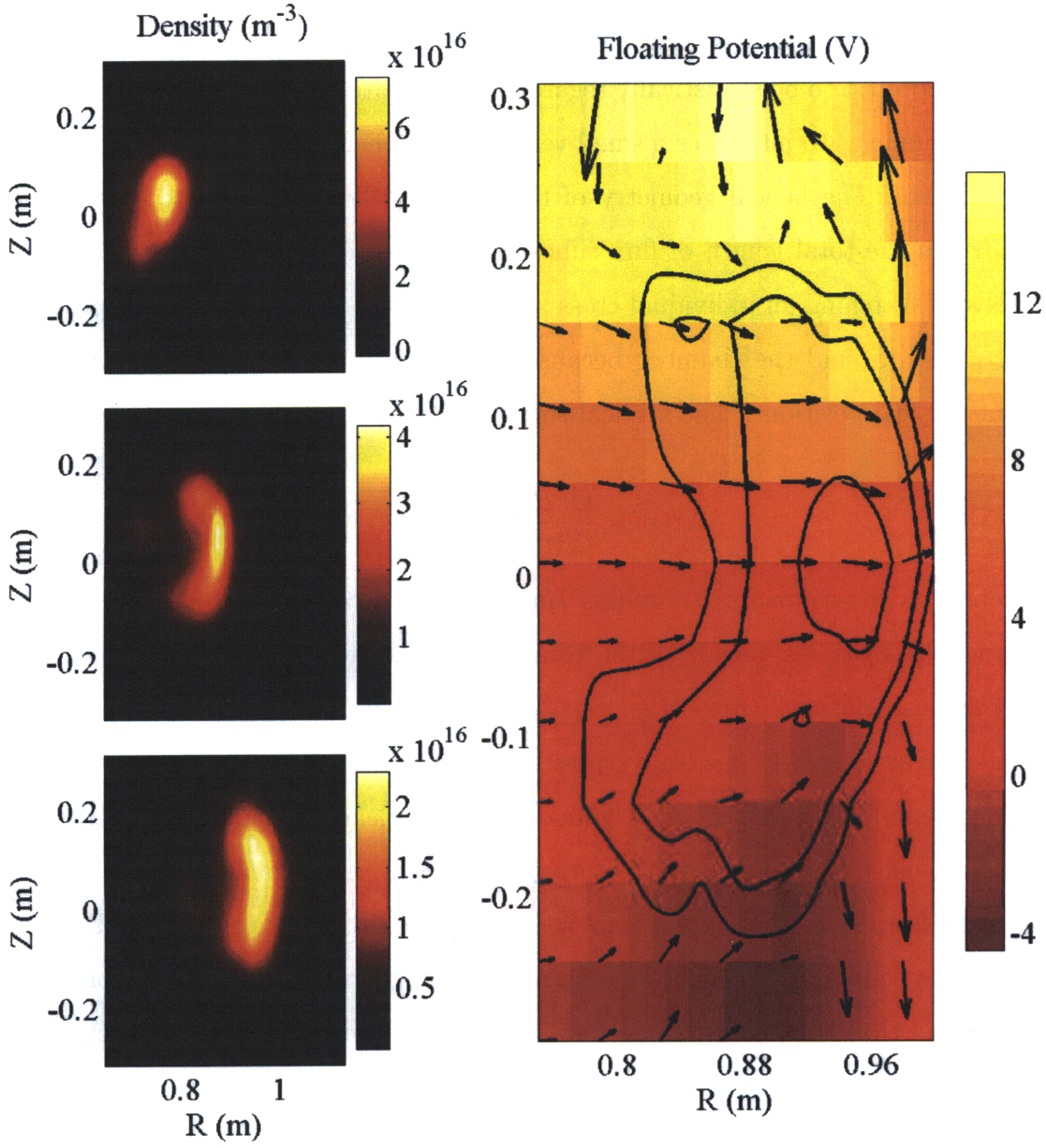

Figure 3-3: This figure is taken from Katz et al [2]. The plot on the right is the cross sectional data of the plasma density and electric field as measured by Langmuir probes. The shading is the plasma potential; the contours are isosurfaces of plasma density. The $\mathbf{E} \times \mathbf{B}$ velocity vectors are shown on the plot. On the left are cross sectional plots of the same blob at three different times. In these frames, the shading is the plasma density.

Chapter 4

Calibration

Using the piezoelectric valve as described in Chapter 2.3, multiple shots were taken, each varying one of the two parameters of neutral gas pressure and vertical magnetic field. The numerical values chosen are listed in Table A in the Appendix. The values had a wide range in order to cover as many physical effects as possible. In particular, the spectrum of neutral gas pressure includes low values for which radial speed near the sound speed was observed for symmetric blobs.

4.1 Timing

In addition to the neutral gas pressure, the timing of the piezoelectric valve and the microwave source was manipulable. As discussed in Chapter 3.3.2, the times we were interested in were on the order of 1ms (radial propagation limit). Due to mechanical constraints on the piezoelectric valve, the shortest duration for the gas puff release was 1ms. A consequence of the valve time and the radial propagation duration being on the same order was that precise timing in the shot process became fundamentally important. Included in the timing considerations was when to begin and when to

finish the microwave source input. If the microwave source is active for too long, the radial propagation and plasma ionization will overlap significantly, which would result in a blob on the order of the vacuum chamber. When the blob dimensions approach those of the vacuum chamber, the blob dynamics are difficult to determine because propagation times are short. In contrast, a too short microwave burst would produce a weak blob, effectively making the signal to noise ratio poor. Theoretical values for the microwave burst time, Δt_μ, and its delay from the beginning of the gas puff, Δt_p, are difficult to predict; the values are best determined by empirical methods. A plot of signal versus time shows the relative positions of Δt_μ and Δt_p in Figure 4-1.

4.1.1 Microwave Burst

To determine the best timing, we conducted a series of calibration shots on October 29 and 30. The values of Δt_μ and Δt_p were varied independently. Initially, the focus was on finding an optimal microwave burst duration. This calibration was performed with plasma created by the interior coil method described in Chapter 2.2 instead of using the piezoelectric valve. A sequence of thirty four shots were taken, although several had redundant parameter values. This sequence of shots probed a wide range of microwave burst durations, 35-200 microseconds. A good burst duration was determined to be 55 microseconds. This value was found by examining the signal to noise ratio and average blob size, which independently provide a way to quantify the extreme cases of too short or too long a microwave burst.

4.1.2 Delay

Adopting 55 μsecs as the standard for microwave burst duration, we focused next on calibrating the timing between the piezoelectric valve and the microwave source. In the piezoelectric model, the background is initially populated by a variable neutral

density. Because no interior coil is used, the background toroidal field must be 87 mT. Consequently, irradiation by microwaves would ionize the background neutrals approximately equally and no asymmetric blob would be created. In order to establish asymmetry, the piezoelectric valve allows neutral Argon gas into the chamber at a specific toroidal angle. This local increase in neutral density needs time to spread. The importance of delaying the microwave burst lies in allowing the neutral gas cloud to occupy a sufficient volume. If the microwave burst is initiated too soon after the piezoelectric valve is activated, then the neutral gas asymmetry will be small. A delay that is too long will allow the neutral gas puff to spread throughout the chamber and effectively become undetectable relative to the background density. Taking these limits into account, a delay of $\Delta t_p = 845\mu$secs produced a good blob. The values of $\Delta t_\mu = 55\mu$secs and $\Delta t_p = 845\mu$secs were used for all data collection shots.

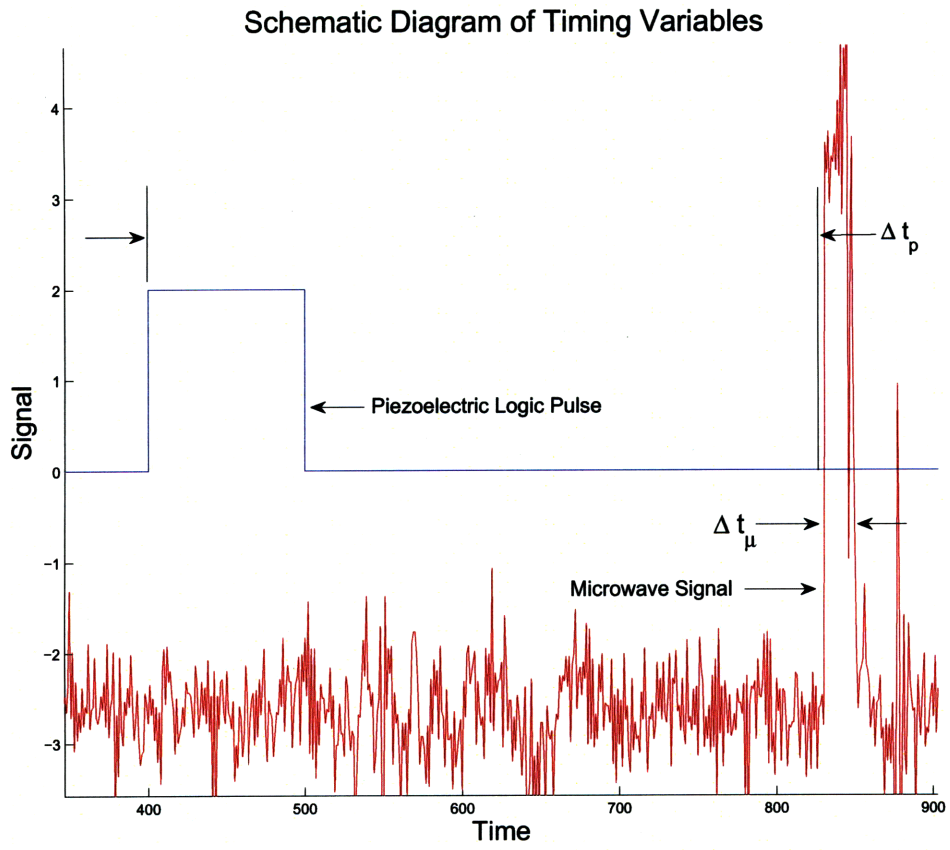

Figure 4-1: The superposition of signal versus time traces for piezoelectric valve and microwave duration shows the relative positions of Δt_μ and Δt_p. In this diagram, the blue trace is a representation of the piezoelectric logic pulse. The red trace is the microwave strength signal. The time from the beginning of the piezoelectric pulse to the beginning of the microwave burst defines Δt_p. The duration of the microwave burst is Δt_μ.

Chapter 5

Data

Each probe of the four Langmuir arrays recorded ion saturation. Because the four toroidal cross sections spanned 100 degrees, toroidal numerical interpolation in space and time was useful to investigate the three dimensional behavior. Two dimensional interpolation at every toroidal cross section aided the search for radial propagation. Spatial interpolation provided continuation throughout the arc of the chamber under investigation. Temporal interpolation helped to smooth out the effect of having unmeasured space due to the physically distinct probes in each array. By focusing on the time intervals immediately after the microwave source is turned off, the blob dynamics were measured. In this thesis, I will describe the results of analyzing the data for radial and toroidal propagation. I find it useful to examine the asymmetric radial speed in detail, including comparison to symmetric blobs, prior to investigating toroidal propagation. Although the two velocities, radial and toroidal, are not necessarily independent of one another, the results from the radial data facilitate discussion of toroidal data.

5.1 Radial Propagation

5.1.1 Radial Propagation Data

When looking for global radial behavior, it is useful to organize the data into a top-down point of view. This is achieved by averaging over the z dimension for all four Langmuir arrays. The remaining variables are the radius and toroidal angle, which are numerically interpolated over. A representative example of the data is plotted in Figure 5-1. A movie of this shot shows the band of plasma density propagate radially. To find the radial speed, it is best to average over the vertical dimension and retain the radial and toroidal variables.

Radial propagation was observed in all asymmetric blobs created with the piezoelectric method (Chapter 2.3). This was determined by looking at the probe measurement as a function of radial position and time step. A representative trace of probe signal versus time step is shown in Figure 5-2. The peak of the curve is interpreted as the blob moving past the probe. A single probe is not sufficient to determine direction and speed; we need the array of probes to specify both. An example of how the array of probes shows blob motion may be seen on a superposition of several signal versus time traces, as shown in Figure 5-3. Although Figure 5-3 provides a qualitative view, a standard procedure is required for calculating the quantities of interest.

In order to extract a radial position, it is necessary to have a quantifiable procedure for determining the location of the blob at any given time step. The natural approach was to calculate the center of mass by spatially interpolating data between probes. A center of mass is most relevant if computed individually for a given toroidal cross section. Because we were interested in the radial behavior, the array of probes was averaged over the z dimension at each radial position. The result was a quantity that is dependant only on the time and radial variables. Taking the time derivative of

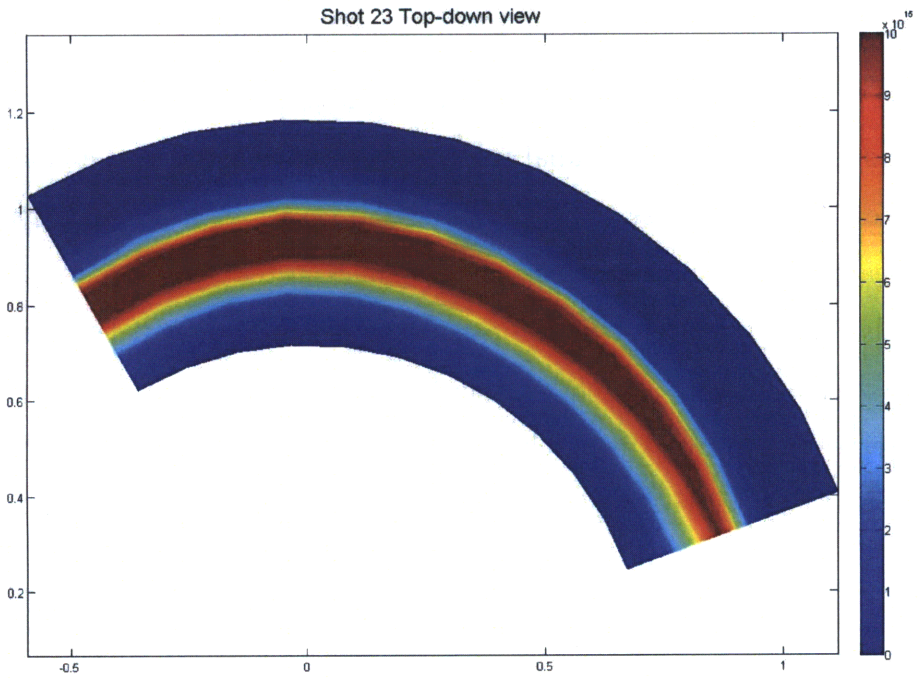

Figure 5-1: Top-down view of data from shot 23. $B_z = 0$ and the neutral gas pressure is 25.2 e-5 Torr. The blob appears as a distinct band as interpolated across the 240-340 toroidal angles.

the radial center of mass numerically yielded the radial velocity. This was computed for each of the four toroidal cross sections available. A representative trace of the calculated radial velocity versus time is shown in Figure 5-4. The negative slope of this plot is indicative of a gradual slowing of the blob's radial propagation. Several mechanisms for blob slowing were discussed in Chapter 3.2. For data analysis it is useful to extract an average radial velocity. An average velocity is a good characteristic to use for comparing how changes in the shot parameters affect the physics of the blob motion.

We note that some interesting features of the plot in Figure 5-4 include the be-

havior at the beginning and at the end of the data collection. These times correspond to the blob at the inner and outer walls, respectively. The blob's interaction with the chamber walls introduce effects that pollute the pure radial propagation regime. These effects interfere with the radial velocity calculation because they may change the computed center of mass. By distorting the center of mass calculation, it is no longer reasonable to interpret the blob dynamics in terms of radial propagation. Consequently, the first action taken in calculating an average radial velocity was to exclude the very beginning and end of the shot. This is an acceptable simplification because it serves to separate the purely propagating regime from the wall effects. The superposition of augmented data sets is shown in Figure 5-5.

The remaining measurements pertain to the blob passing through the radial center of the vacuum chamber. In fact, it is possible to track the blob's general radial position by counting the number of local maxima passed. These local maxima are an artifact of the data interpolation due to the radial spacing between hanging probes. The calculation of the center of mass is unavoidably biased towards positions around probes. As the real blob passes between probes, the data show a sudden decrease in the total plasma density. This is because there is no probe to measure the real blob in the empty region. The lower density changes the weighting in the center of mass calculation. As the blob begins to interact strongly with the next probe on its outward movement, there is a sudden increase in signal at the new probe's location. In effect, the center of mass calculation "jumps" to the following probe. This computational artifact does not entirely mask the physical behavior of the blob propagation; however, it is an effect that needs to be taken into account in the error analysis.

5.1.2 Radial Propagation Error Analysis

I have discussed the motivation for removing data from the very beginning and end of the shot (Chapter 5.1.1 and Figure 5-4). A more detailed explanation is required for understanding the local maxima in the velocity versus time plot of Figure 5-5. A strictly physical interpretation of the local maxima would be the existence of a radially directed, time dependent force that alternately accelerates the blob outwardly and inwardly. There is no physical basis for such a force to exist; consequently, a procedure must be developed for analytically determining how the errors affect the velocity calculation.

Interpolation in time helped to reduce the effect of dead space between probes. It was discovered that the optimal window of time steps should be chosen by individual inspection. From this window, which was typically 100 time steps, a mean was directly calculated. To establish confidence bounds, this window was either shifted or changed in size. For every change, the average velocity was recomputed. A value was considered robust if the difference between the maximum and minimum was under ten percent of the mean value. The results are given in Table 5.1.

These results may be plotted on a log-log graph, which is shown in Figure 5-6. This plot clearly shows that the radial velocity has a dependence on the neutral gas pressure. The linear nature of this curve is indicative of a $\frac{1}{P_n}$ relationship between velocity and neutral pressure P_n. This behavior will be compared with the symmetric blob case later in Chapter 5.2.1.

Table 5.1: Average radial velocity for asymmetric blobs. Includes results for shots taken with different z components of magnetic field.

Shot	Neutral Pressure (10^{-5}) Torr	B_z mT	Velocity in m/s	± Error in m/s
14	6.02	0	2030	252
17	9.66	0	1242	127
20	15.4	0	535	35
23	25.2	0	525	48
26	33.6	0	381	15
29	43.4	0	374	33
32	0.448	0	2731	2400
15	6.02	2.02	320	65
18	9.66	2.02	221	37
27	33.6	2.02	175	20
30	43.4	2.02	81	22

5.2 Comparison

5.2.1 Symmetric Blob Results

The results shown in Figure 5-4 may be directly compared to the observations of symmetric blob radial propagation investigated by Katz et al [2]. Under a similar range of neutral pressures, the authors found a scaling of velocity with pressure. The results are listed in Table 5.2.

It is of interest to compare the radial speed of asymmetric blobs versus symmetric blobs. The relevant numbers are summarized in Figure 5-7. This plot shows that when the B_z component is zero, radial speed of asymmetric and symmetric blobs is similar to within confidence bars. As the $\mathbf{e_z}$ component of the magnetic field becomes nonzero, the blob speeds diverge, with slower average speed for nonzero B_z. An interpretation of this behavior will be discussed in Chapter 5.2.2.

Table 5.2: Results of symmetric blob radial average velocities as found by Katz et al [2]. B_z is zero for all shots.

Neutral Pressure (10^{-5}) Torr	Velocity in m/s	$\pm$ Error in m/s
4.118	2705.3	428
5.68	2226.4	471.2
7.2420	1667.9	296
8.5200	1944.4	257.5
9.9400	1561.4	262
10.9340	1804.0	250
11.0760	1378.9	264.1
12.9220	1078.9	309.1
14.0580	984.7	315.9
21.3000	884.3	475
21.3000	780.4	305.7
22.7200	988	250
28.4000	615.3	352.4
36.9200	471.2	351.5
45.4400	373.4	281.4
45.4400	401.9	189.4
45.4400	398.7	204.9

5.2.2 Physical Interpretation of Results

It is clear from Figure 5-7 that the B_z component has a greater impact on radial speed than toroidal symmetry/asymmetry does in the experiment. There is a qualitative explanation for this behavior that originates from the fact that charged particles follow flux tubes. In the absence of a vertical magnetic field component, flux tubes are confined in the $\mathbf{e_z}$ direction. Except for the effect of toroidal asymmetry by design, there is no relationship between the toroidal angle and $\mathbf{e_z}$ dimension. For symmetric blobs, their flux tube forms a continuous toroid within the vacuum chamber. Asymmetric blobs experience no propagation in the $\mathbf{e_z}$ direction; their toroidal propagation goes about the inner wall and connects onto itself. Vertical charge separation proceeds according to the dynamics discussed in Chapter 3.1, which leads to the $\mathbf{E} \times \mathbf{B}$ radial drift.

When a $\mathbf{e_z}$ component to the magnetic field is introduced, the flux tubes change shape to follow the field lines. Instead of a ring, the flux tube resembles a helix (see Figure 5-8).

Particles move along magnetic field lines. Because of the B_z component, particles can change their z position and the $\nabla_{||} J_{||}$ term in Equation 3.13 becomes important. The charge separation in toroidal cross sections can be affected by charged particles moving from other cross sections. The vertical electric field that arises due to gradient and curvature drift can now be shorted by hot electrons flowing up the magnetic field lines from other toroidal angles. This will reduce the magnitude of the electric field. In turn, the $\mathbf{E} \times \mathbf{B}$ drift will be proportionally less. This explanation is helpful for predicting some of the possible features that toroidal data will show. In particular, the fact that B_z affects the average radial speed is a statement about the rate of toroidal propagation. In order for the hot electrons to short the electric field, they will need to propagate throughout the asymmetric blob. Because the average radial

speed is significantly reduced in the presence of a nonzero B_z due to currents shorting the electric field, we expect to see significant toroidal flow.

5.3 Toroidal Propagation

5.3.1 Toroidal Propagation Data

The four Langmuir arrays used in this experiment were spread over toroidal angles 240, 270, 300, and 340. Each array yielded a good measurement of the plasma activity within the toroidal cross section. In analyzing the toroidal data, we investigated the measurements at each of the four cross sections in conjunction with one another. The relative plasma densities could be used to watch for toroidal propagation. Because the flux tube passes through the four cross sections, the flow of particles will obey the continuity equation within some subset of the total vacuum chamber cross section. Namely, it is not necessary to observe the plasma density across the entire cross section; tracking the actual flux tube should be possible. By comparing the relative density of the flux tube at the four cross sections, we can track toroidal motion of the blob.

Some representative cross sectional views are shown in Figure 5-9. This figure shows cross sectional plots of the same blob at different times. The high density blob is clearly seen to be at the same radial location for each of the cross sections. This is a confirmation that the feature is indeed the same blob as viewed over 100 degrees toroidally. The blob shown in Figure 5-9 was created in the absence of a vertical magnetic field component. Analysis described in Chapter 5.1.1 produced an average radial speed that is within confidence bars of the symmetric blob results of [2]. By watching a movie of its radial propagation in the toroidal cross section, we saw that the blob's behavior closely resembled that of the symmetric blob in Figure 3-3. This

is not surprising considering that this blob was created under very similar conditions to those in which the symmetric blobs were measured.

A more interesting study was to investigate the toroidal cross sections for shots which had a nonzero vertical magnetic field. Numerical results in Table 5.1 show very dissimilar values for asymmetric blobs in the presence or absence of B_z. Because the data presented in that Table were averaged over the z coordinate, some of the behavior due to the nonzero B_z was ignored. In particular, by averaging over z, we focused on the toroidal dynamics; here, we want to look at the vertical changes. Equation 3.3.2 is a prediction of the relationship between the radial and vertical positions of a blob that originates from the requirement that plasma stays within the flux tube. A cross sectional view of a blob in a vertical magnetic field can be used to test this relationship. Figure 5-10 shows a blob with a nonzero B_z at different times. The blob quickly begins to fragment into several islands of plasma density. These islands are seen to propagate diagonally to form fingerlike structures (see Figure 5-11).

Examination of Figure 5-11 is convincing evidence that the fingerlike structures are distinct structures. To extract some toroidal information, it is necessary to compare the four different cross sections. Differences between the cross sections is indicative of toroidal variation. Figure 5-13 shows shot 19 on the four cross sections at the same time. The four cross sections all exhibit the same shape of fingerlike plasma projections. If there were a difference in the densities of the projections that appeared in the sequence of toroidal angles, then the change would be due to a toroidal "wavefront" of plasma that is flowing toroidally. This toroidal variation in density could be tracked through time to find a flow rate. Numerical examination of the data in Figure 5-13 and similar shots did not reveal any significant density change over the four cross sections. Thus, the fingerlike extensions are simply the outward propagation of fully extended helical flux tubes that were created by hot electrons during the microwave ionization stage.

During the microwave ionization stage, hot electrons traversed the chamber several times toroidally and ionized a complete flux tube. Once the microwave source was shut off, the entire flux tube began to propagate outward. Evidence of the flux tube during ionization is shown in Figure 5-12.

The helical flux tube would undergo outward propagation over the duration of the shot. Due to the vertical magnetic field component, the upper and lower branches of the helix would spread along a parabolic path according to Equation 3.18 as viewed in a cross section. The diagonal fingers in Figure 5-13 approximately obey this parabolic relationship between radius and vertical height. This is additional evidence that the fingerlike projections are the cross section intersections with the outward propagation of the helical flux tube.

An interesting feature to look at is the confinement of the fingerlike projections. In Figure 5-11, they appear to be strongly localized around individual probes. Although this is certainly a feature of the interpolation scheme, it is clear from that figure that the projections are thin in the vertical direction. This is compared to the plot of Figure 5-9 in which there was no B_z component. In the latter figure, the blob is spread vertically across approximately 40 cm as opposed to the projections that have a vertical spread of about 10 cm. This behavior is currently not understood and serves as a good focus for future research.

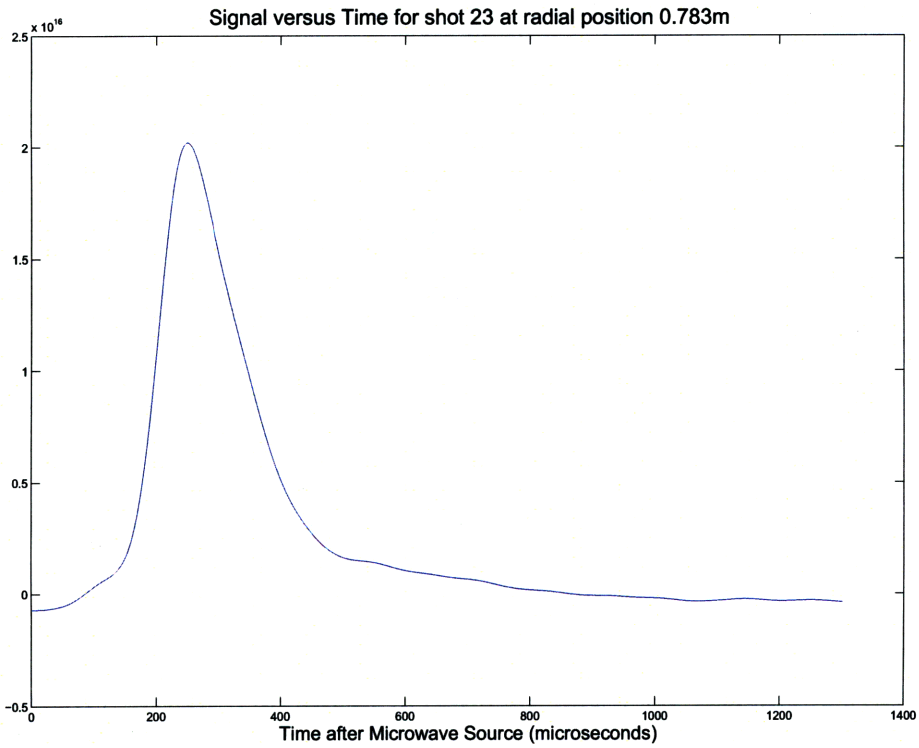

Figure 5-2: Signal versus time step plot of Langmuir probes for shot 23. The asymmetric blob was created with the piezoelectric valve and without a z component magnetic field. The data shown in the trace were collected by probes at radial position 0.783m for the 240 cross section array. The measurements were averaged over the vertical dimension. The peak of the curve corresponds to the blob's center of mass (at this toroidal cross section) passing the probes' radial location. Direction of motion and speed are determined by using several probes in conjunction.

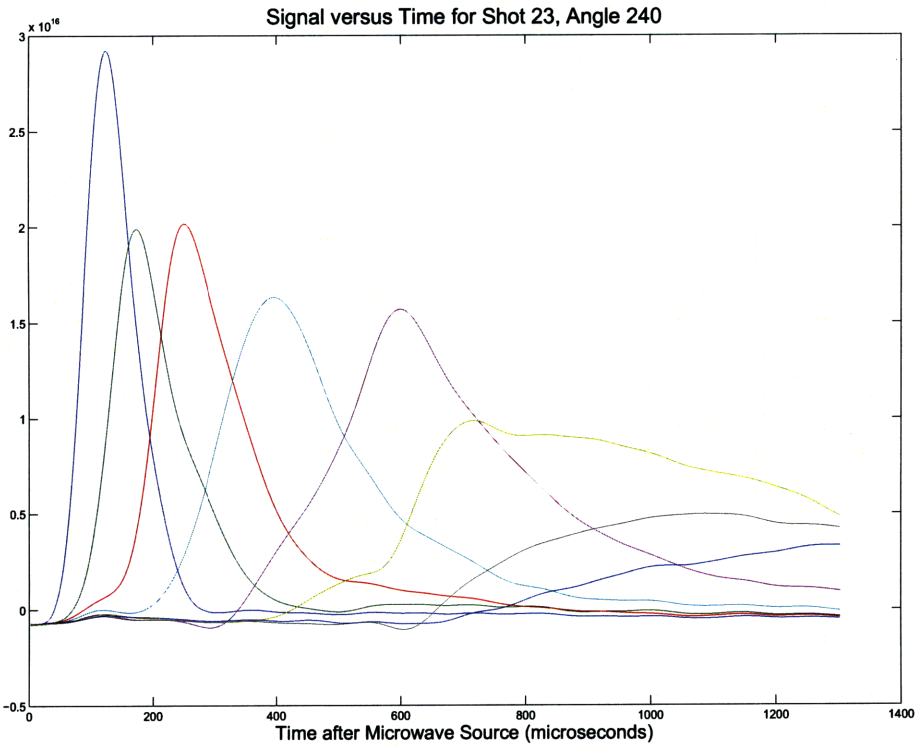

Figure 5-3: This plot shows the superposition of signals from several probes at angle 240 cross section versus time for shot 23. The z component of the array has been averaged over such that the relevant spatial dimension is radial. Different radii correspond to different traces. $B_z = 0$ mT for this shot and the measurements are recorded after the microwave source has been shut off. The order of signal peaks is indicative of radially outward motion.

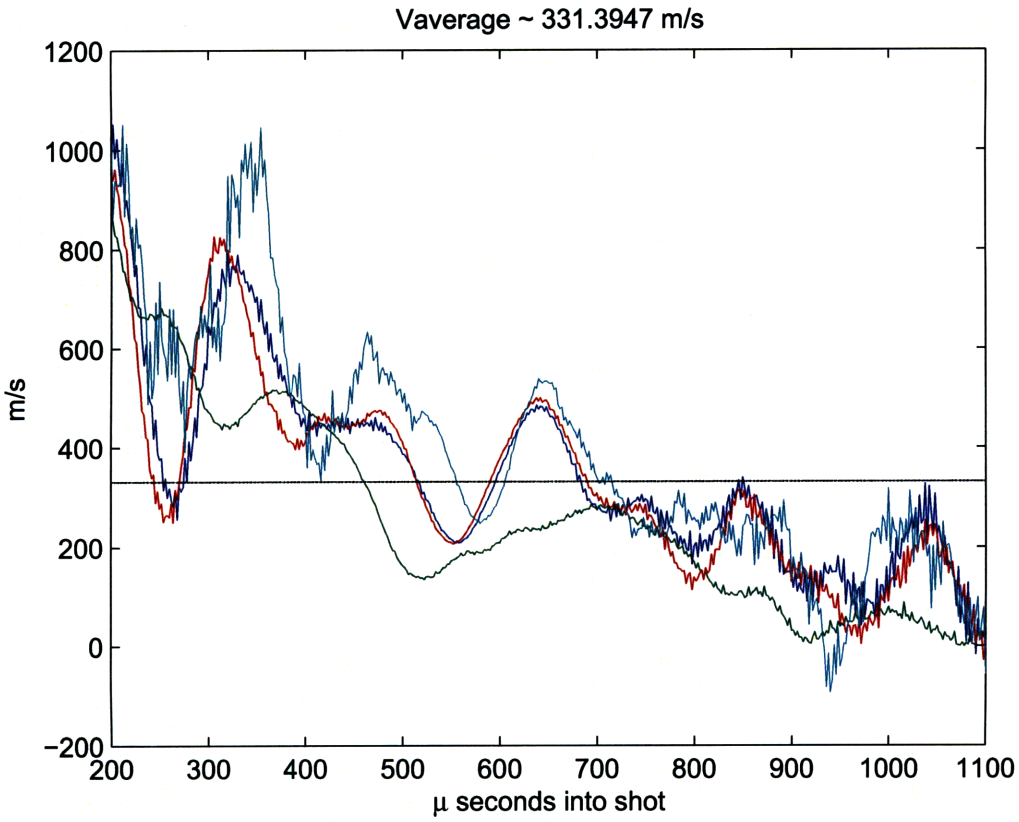

Figure 5-4: Radial velocities versus time for the four cross sections of shot 23. The large variation in radial speed near the beginning and the end of this plot shows the errors due to the blob interacting with the inner and outer wall, respectively. The average computed speed for this subset of time steps may be compared with the value attributed to shot 23 shown in Table 5.1.

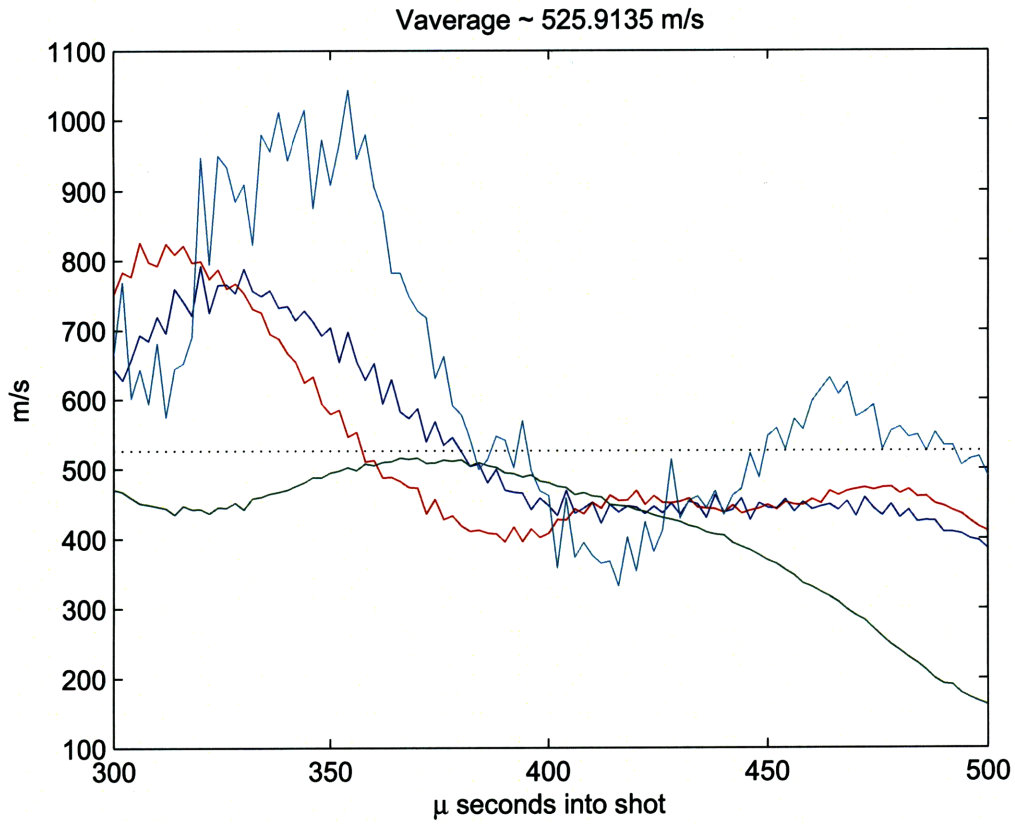

Figure 5-5: This shows the trace in Figure 5-4 reduced by excluding the beginning and end of the shot. The remaining data corresponds to the blob traveling through the radial center of the chamber.

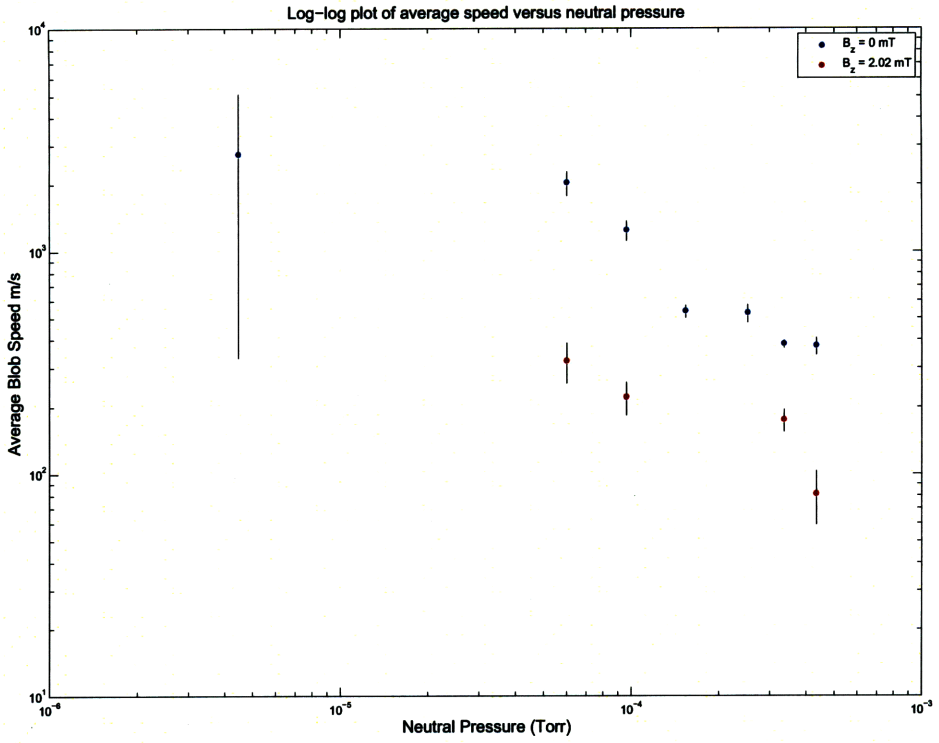

Figure 5-6: Log-log plot of average speed versus neutral pressure for several different pressure and B_z magnetic fields. The neutral pressure indicated is the pressure in the vacuum chamber prior to the injection of Argon gas through the piezoelectric valve.

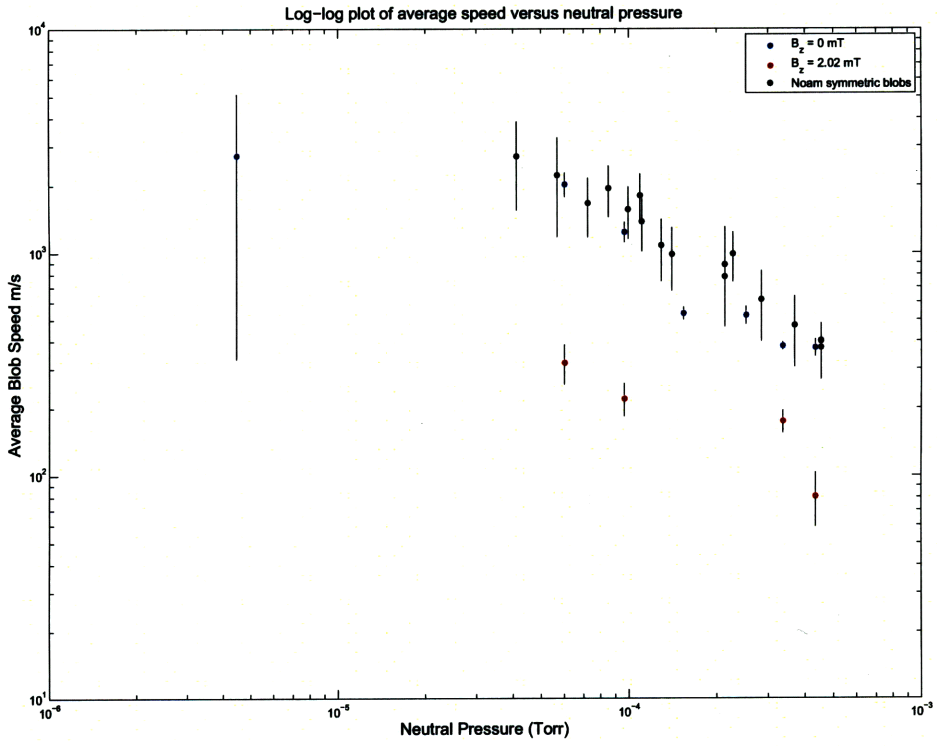

Figure 5-7: Log-log plot of average radial velocity versus neutral pressure. Comparison between symmetric and asymmetric blobs reveals that a B_z component was more significant than toroidal symmetry.

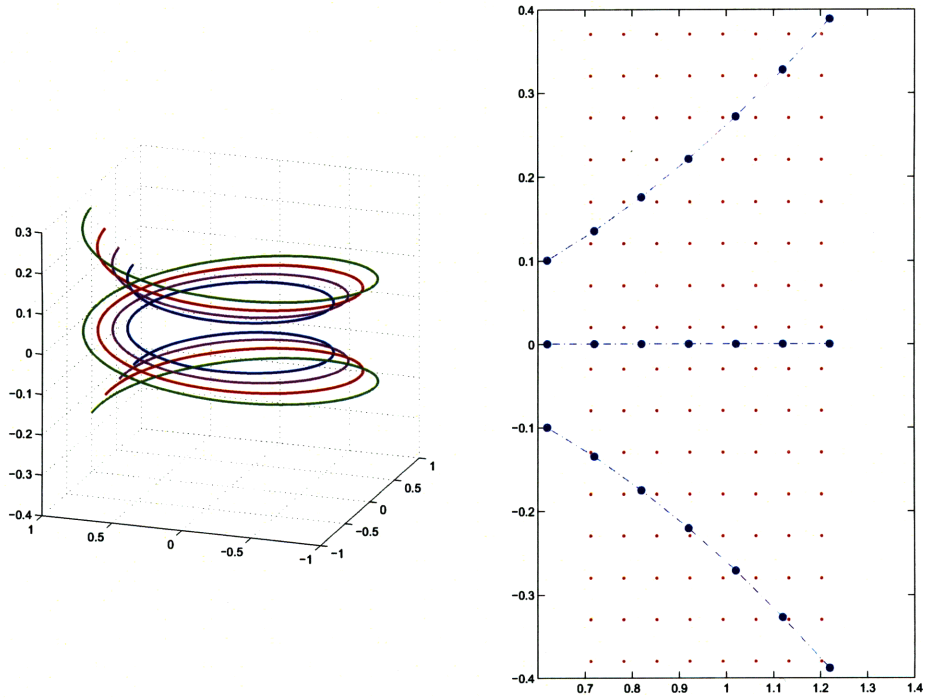

Figure 5-8: On the left is a schematic drawing of the magnetic field lines. The different colors are the magnetic field lines at different radii. Notice the vertical spread of the helixes based on the radius. The plot on the right features the Langmuir probe array in red as it would be spaced at toroidal angle 240. The blue dots are the intersections of the some different field lines. Although these field lines were chosen such that they all intersect the z = 0 line, the vertical spacing between subsequent intersections is a parabolic function of radius, shown as a dashed blue line. A helical flux tube located at the inner wall would appear as several vertically separated patches of plasma density in the cross sectional view. These density islands would drift vertically apart as the flux tube propagates outward. The trajectories that the islands follow obey Equation 3.18 with $B_z = 2.02$ mT and $B_\phi = 48.7$ mT, which are typical values used in the experiment.

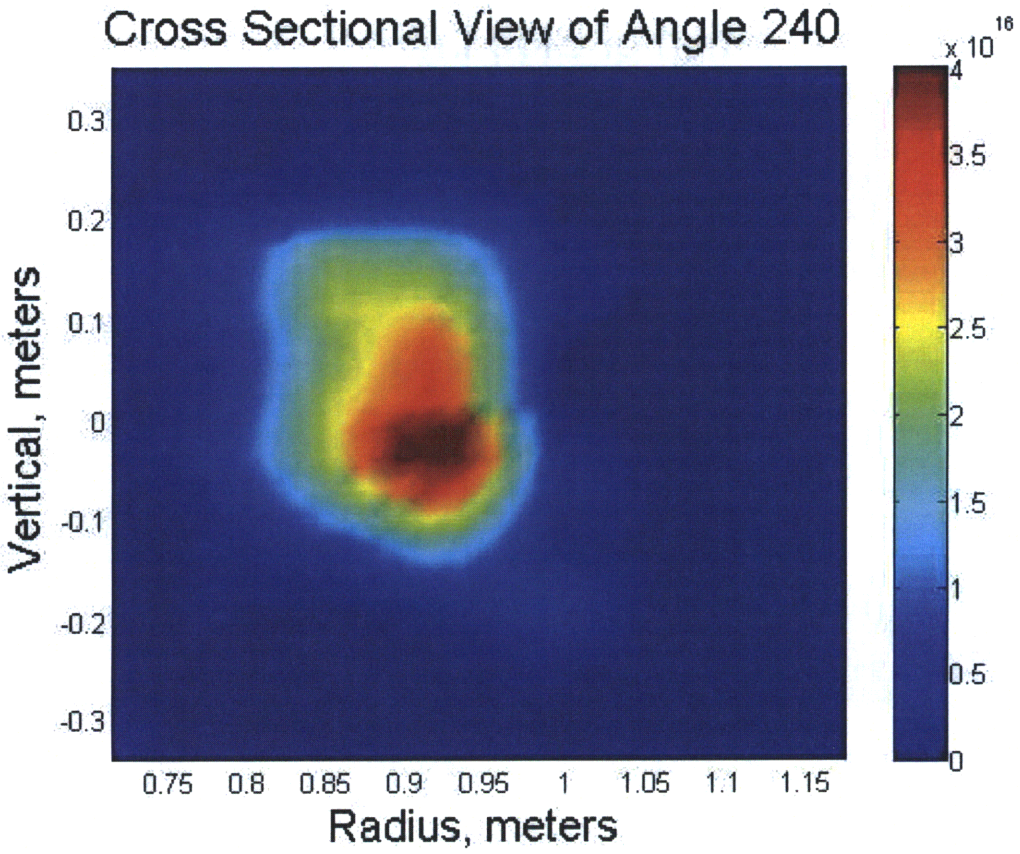

Figure 5-9: Cross sectional views of shot 23 at toroidal angle 240. The B_z component is 0 mT and the neutral gas pressure is 2.82 e-4 Torr. The shading corresponds to plasma density in particles per volume. This plot features interpolated data between probes in the R, Z directions.

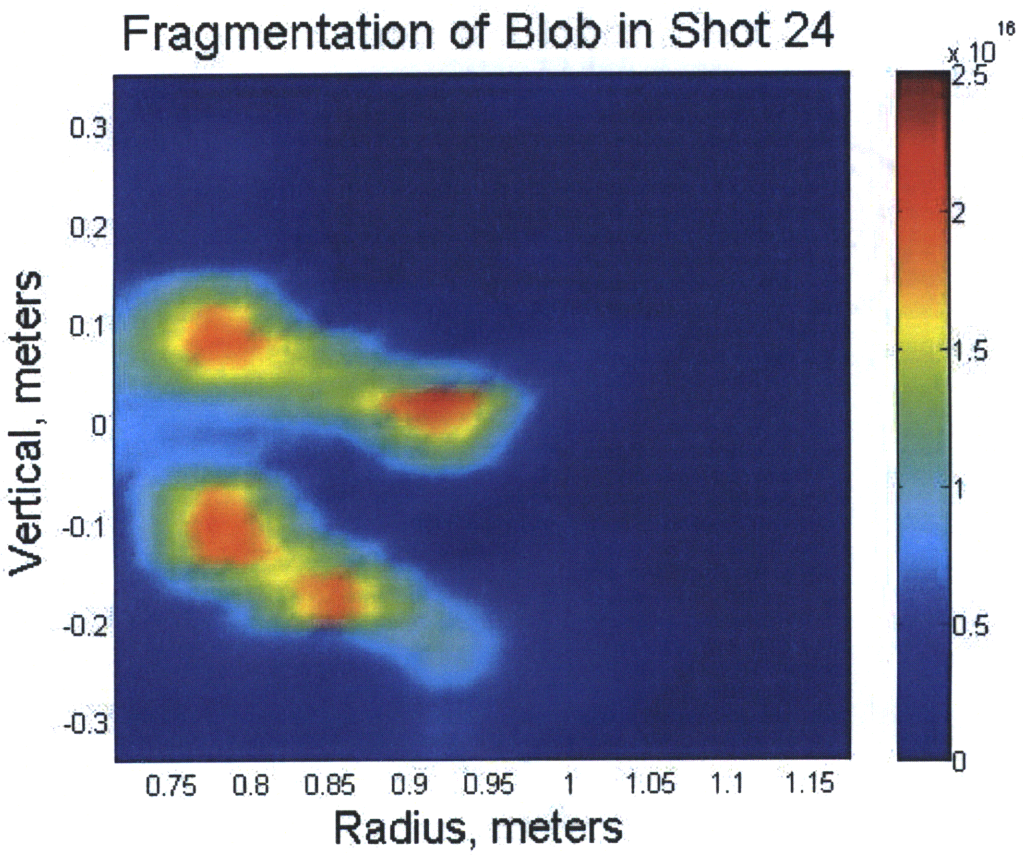

Figure 5-10: Cross sectional views of shot 24. The B_z component is 2.02 mT and the neutral gas pressure is 2.82 e-4 Torr. The shading corresponds to plasma density. The blob is seen to fragment into density islands over the course of the shot. This behavior is not observed in the absence of a vertical magnetic field component.

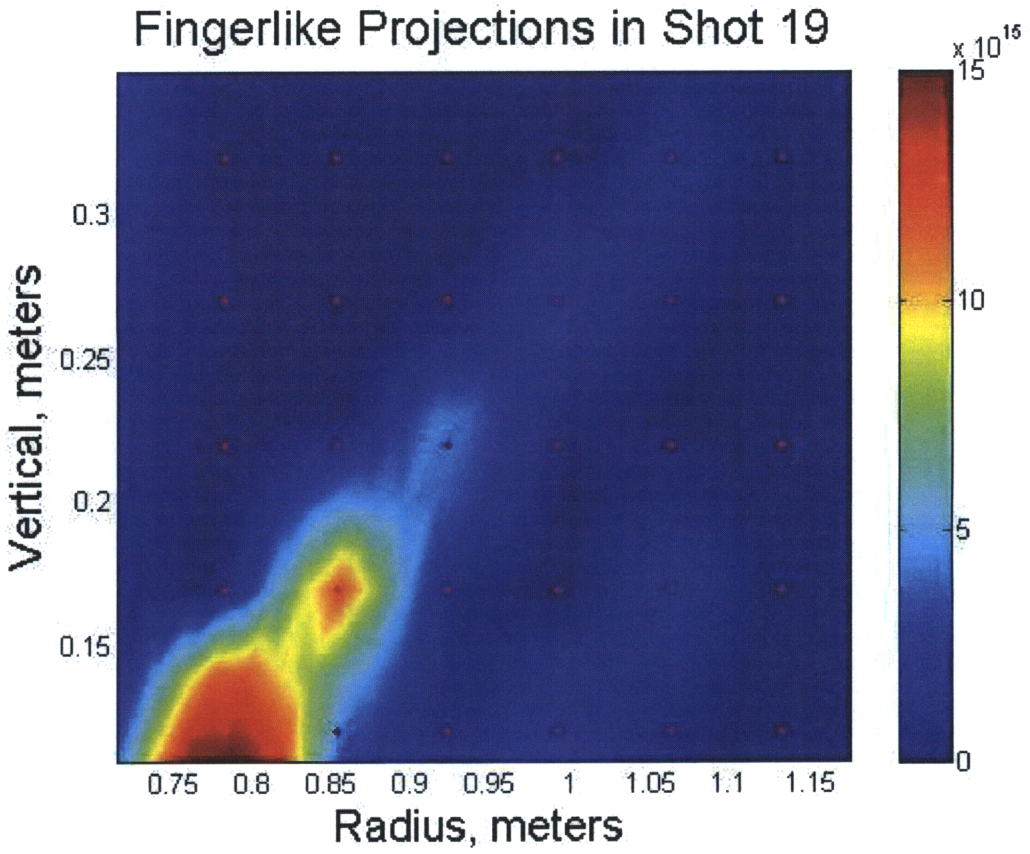

Figure 5-11: Fingerlike extensions of plasma density of shot 19 at a subset of the array. B_z is 4.3 mT and the neutral gas pressure is 9.66 e-5 Torr. The red dots are the Langmuir probes. The fingerlike nature of the plasma extensions is due to the toroidal propagation about the chamber. Numerical interpolation between the probes is clear from looking at the position of the dots; however, the diagonal spread is from toroidal motion.

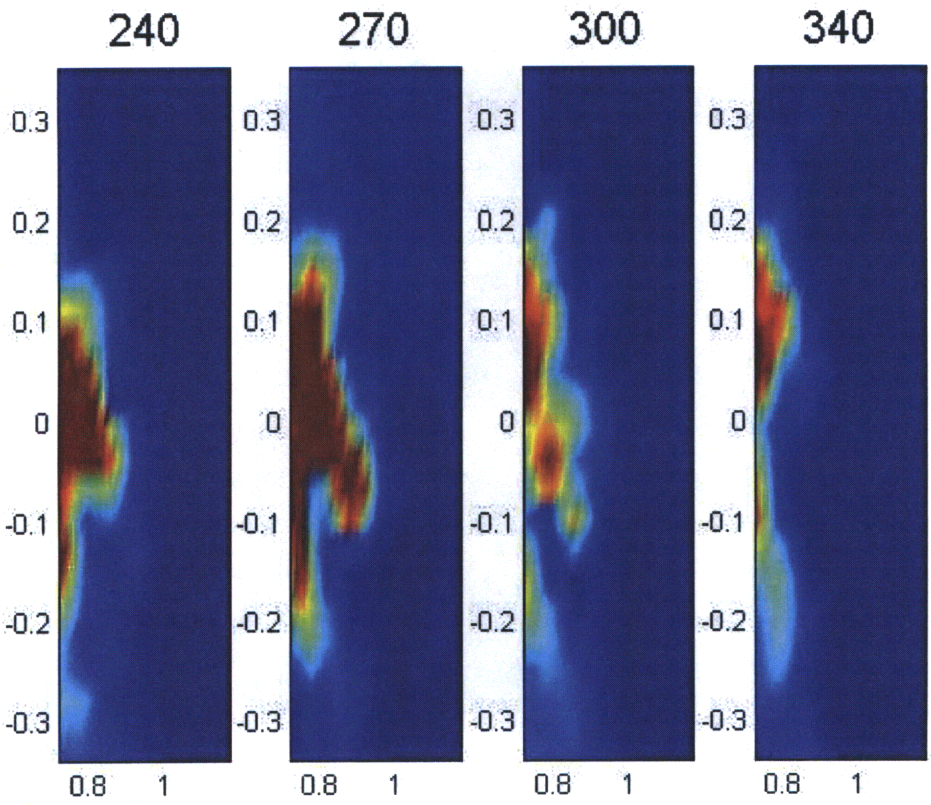

Figure 5-12: Cross sectional views of shot 19 across the four toroidal angles. These frames were captured immediately following microwave shutoff. The thick vertical band near the inner wall is actually several toroidal passes of a flux tube. Compare these plots with the vertical spread in Figure 5-9.

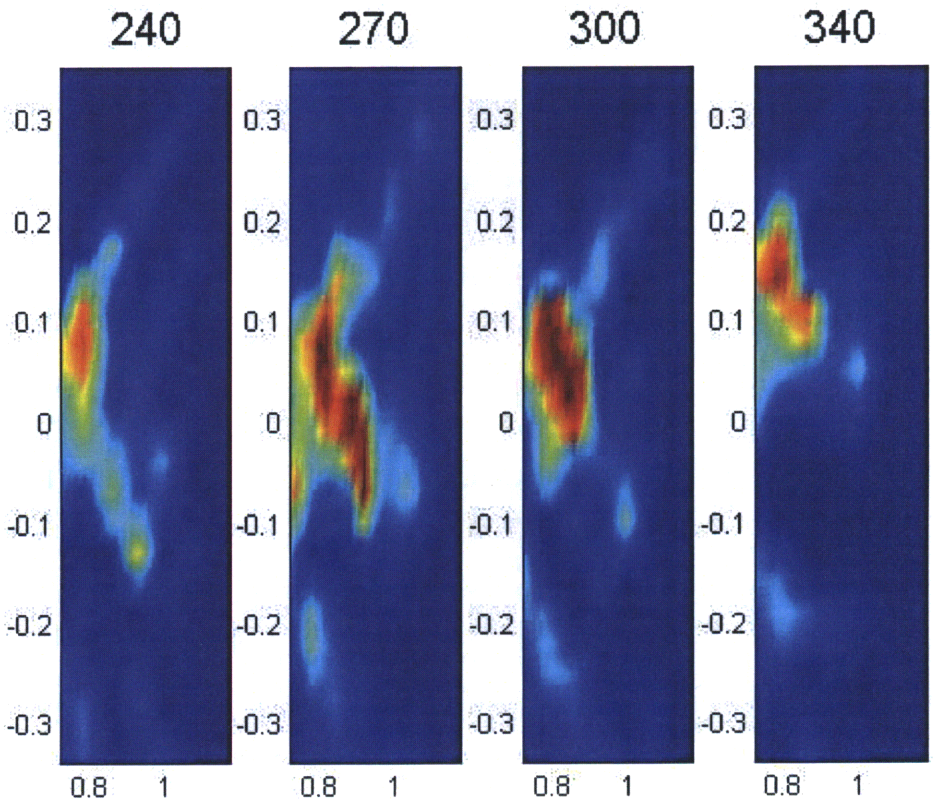

Figure 5-13: Several fingerlike plasma projections are seen over the four toroidal angles for shot 19. B_z is 4.3 mT and the neutral gas pressure is 9.66 e-6 Torr. The vertical separation of these projections is close to the predicted vertical offset of the magnetic field lines per single toroidal revolution about the chamber. Although the fingers are distinct, they appear to originate from the inner wall at the beginning of the shot, which points to the idea that the asymmetric blob was fully extended toroidally during the ionization stage.

Chapter 6

Conclusions

This thesis has covered the the major phases of an experiment designed to investigate the dynamics of asymmetric plasma blobs, from setup to interpretation of results. Notably, I explained the various techniques by which asymmetric blobs could be created. Two designs, an inside perturbation coil and piezoelectric valve, were tested. Although the perturbation coil functioned, its geometry was not optimized for the vacuum chamber. Thus, the piezoelectric valve was used to create asymmetric blobs. This setup yielded several interesting observations.

We looked at the data collected from four arrays of Langmuir probes that covered a range of 100 degrees toroidally around the chamber. The four cross sections yielded both radial and toroidal information about the plasma blob. The average radial velocities had an inverse dependence on neutral gas pressure. Comparison with symmetric blob data taken by previous students at VTF [2] showed that the asymmetric nature of the blob was less important than a B_z magnetic component. A small vertical magnetic field significantly changed the average radial speeds.

Torodially, the blob did not appear to propagate. Our interpretation of the data is that the blobs were already fully extended into several loops around the inner wall

when the microwave source was shut off. The microwave source excited hot electrons that ionized a helical flux tube about the inner wall. The propagation observed in the cross sections by the Langmuir probes was the outward motion of the multiple branches of the helical flux tube and not toroidal flows of the blob.

This experiment has also made discoveries that are not yet understood and would be interesting areas on which to focus future research. For example, in addition to changing the radial speed, the presence of a nonzero B_z was observed to confine the vertical dimension of the plasma blob extensions as seen in Figure 5-11. Currently, there is no tested physical explanation for this effect. Future research into the dynamics of asymmetric blob propagation would also benefit from optimization of the engineering aspects of the blob creation and blob measurement. Experiments may want to reinvestigate the use of an inside, perturbative coil to generate asymmetric blobs. Alternatively, VTF students are currently working on an apparatus designed for direct plasma injection into the vacuum chamber. This device would free the experiment from the 87 mT constraint, which would make the toroidal magnetic field another variable to investigate.

As a pioneering experiment on asymmetric blobs, this thesis reveals many of the interesting possibilities that have only just been glanced at. Asymmetric blobs may be fundamental for the future understanding of areas within magnetic reconnection because of the asymmetric, three dimension nature. The study of these blobs has proven to be a fertile area that is both challenging and rewarding.

Appendix A

Data Table

Table A.1: Parameters for shots taken on October 30, 2008. Piezoelectric valve is open for 1 ms in every shot. Microwave source is active for a duration of $\Delta t_\mu = 55$ microseconds for all shots. The lapse between the opening of the piezoelectric valve and the microwave activation is $\Delta t_p = 845$ microseconds. Due to blob fragmentation, it was difficult to determine a radial speed for some shots.

Shot #	Neutral Pressure (10^{-5}) Torr	B_z mT m/s	Radial Speed m/s	Error
14	6.02	0	2030	252
15	6.02	2.02	320	65
16	6.02	4.35	N/A	N/A
17	9.66	0	1242	127
18	9.66	2.02	221	37
19	9.66	4.35	N/A	N/A
20	15.4	0	535	35
21	15.4	2.02	N/A	N/A
22	15.4	4.35	N/A	N/A
23	25.2	0	525	48
24	25.2	2.02	N/A	N/A
25	25.2	4.35	N/A	N/A
26	33.6	0	381	15
27	33.6	2.02	175	20
28	33.6	4.35	N/A	N/A
29	43.4	0	374	33
30	43.4	2.02	81	22
31	43.4	4.35	N/A	N/A
32	0.448	0	2731	2400
33	0.448	2.02	N/A	N/A
34	0.448	4.35	N/A	N/A

Bibliography

[1] J Egedal, A Fasoli, M Porkolab, and D Tarkowski. Plasma generation and confinement in a toroidal magnetic cusp. *Rev. Sci. Instrum.*, 71:3351–3361, 2000.

[2] Noam Katz et al. Experiments on the propagation of plasma filaments. *Phys. Rev. Letter*, 101:015003, 2008.

[3] Ian H. Hutchinson. *Principles of Plasma Diagnostics.* Cambridge University Press, New York, second edition, 2002.

[4] G Le, CS Huang, RF Pfaff, SY Su, HC Yeh, RA Heelis, FJ Rich, and M Hairston. Plasma density enhancements associated with equatorial spread f: Rocsat-1 and dmsp observations. *Geophys. Res. Lett*, 108:1318, 2003.

[5] J Park, KW Min, JJ Lee, H Kil, VP Kim, HJ Kim, E Lee, and DY Lee. Plasma blob events observed by kompsat-1 and dmsp f15 in the low latitude nighttime upper ionosphere. *Geophys. Res. Lett*, 30:2114, 2003.

[6] A. A. Pimenta, Y. Sahai, J. A. Bittencourt, and F. J. Rich. Ionospheric plasma blobs observed by oi 630 nm all-sky imaging in the brazilian tropical sector during the major geomagnetic storm of april 6-7, 2000. *Geophys. Res. Lett*, 34:L02820, 2007.